Mutation Research 665 (2009) 67–74

Contents lists available at ScienceDirect

Mutation Research/Fundamental and Molecular Mechanisms of Mutagenesis

journal homepage: www.elsevier.com/locate/molmut
Community address: www.elsevier.com/locate/mutres

Centrosomal amplification and aneuploidy induced by the antiretroviral drug AZT in hamster and human cells

Jennifer P. Borojerdi[a,1], Jessica Ming[a,1], Catherine Cooch[a], Yvona Ward[b], Cristina Semino-Mora[c], Mia Yu[a], Hannan M. Braun[a], Barbara J. Taylor[a], Miriam C. Poirier[a], Ofelia A. Olivero[a,*]

[a] Laboratory of Cancer Biology and Genetics, CCR, NCI, NIH, Bethesda, MD 20892, USA
[b] Cell and Cancer Biology Branch, CCR, NCI, NIH, Bethesda, MD 20892, USA
[c] Laboratory of Gastrointestinal and Liver Studies, Department of Medicine, Uniformed Services University of the Health Sciences, Bethesda, MD 20814, USA

ARTICLE INFO

Article history:
Received 3 December 2008
Received in revised form 9 March 2009
Accepted 10 March 2009
Available online 24 March 2009

Keywords:
Kinetochore
Aurora A
Aurora B
Immunohistochemistry
Zidovudine
Flow cytometry
Confocal microscopy
Pericentrin

ABSTRACT

The centrosome directs chromosomal migration by a complex process of tubulin–chromatin binding. In this contribution centrosomal abnormalities, including centrosomal amplification, were explored in Chinese hamster ovary (CHO) and normal human mammary epithelial cells (NHMECs) exposed to the antiretroviral drug zidovudine (3′-azido-3′-deoxythymidine, AZT). Centrosomal amplification/fragmentation was observed in both cell types and kinetochore positive micronuclei were found in AZT-exposed CHO cells in correlation with dose. Normal human mammary epithelial cell (NMHEC) strain M99005, previously identified as a strain that incorporates high levels of AZT into DNA (high incorporator, HI), showed greater centrosomal amplification when compared with a second strain, NHMEC M98040, which did not incorporate AZT into DNA (low incorporator, LI). Additionally, an abnormal tubulin distribution was observed in AZT-exposed HI cells bearing multiple centrosomes. Immunofluorescent staining of human cells with Aurora A, a kinase involved in the maturation of the centrosome, confirmed the induction of centrosomal amplification and revealed multipolar mitotic figures. Flow cytometric studies revealed that cells bearing abnormal numbers of centrosomes and abnormal tubulin distribution had similar S-phase percentages suggesting that cells bearing unbalanced chromosomal segregation could divide. Therefore, AZT induces genomic instability and clastogenicity as well as alterations in proteins involved in centrosomal activation, all of which may contribute to the carcinogenic properties of this compound.

Published by Elsevier B.V.

1. Introduction

The centrosome is an organelle that regulates migration of chromosomes to the daughter cells, and is also a microtubule organizer. Based on the multiple proteins residing in the centrosome-associated protein matrix, centrosomes have been implicated in other cellular functions including cell-cycle transitions, such as G_1 to S-phase, G_2 to mitosis and metaphase to anaphase [1,2]. Cells normally have one centrosome, which duplicates synchronously with the phases of the cell cycle to generate two new centrosomes, each of which is comprised of a pair of orthogonally placed centrioles. Inhibition of centrosomal duplication generates incomplete mitotic spindles lacking cell polarity. Conversely, a multiplicity of centrosomes will generate aberrant mitotic spindles with chromosomes migrating to numerous poles, hence causing aneuploidy. Most human carcinomas have an abnormal centrosomal number that contributes to the genomic instability characteristic of transformed cells [3–6]. Additionally, it has been reported that malfunction of the centrosome induces delay in the G_1–S progression of the cell cycle [7,8].

Zidovudine (3′-azido-3′-deoxythymidine, AZT), the first nucleoside reverse transcriptase inhibitor (NRTI) used for HIV-1 therapy has been shown to induce micronuclei, chromosomal aberrations, mutations and telomeric attrition *in vitro* and *in vivo* [9,10]. Additionally AZT becomes incorporated into eukaryotic DNA [11,12] and induces cell cycle arrest with accumulation of cells in S-phase [13–17]. Since AZT has been shown to be a transplacental car-

Abbreviations: AZT, azidothymidine, 3′-azido-3′-deoxythymidine; BSA, bovine serum albumin; CHO, Chinese hamster ovary; CREST, calcinosis, Raynaud phenomenon, esophageal dysmotility, sclerodactyly, and telangiectasia; DAPI, 4′,6-diamidino-2-phenylindole dihydrochloride; LI, low incorporator; HI, high incorporator; IHC, immunohistochemistry; NHMEC, normal human mammary epithelial cell; NRTI, nucleoside reverse transcriptase inhibitor; PBS, phosphate buffer saline; TBS, Tris buffer saline; TEM, transmission electron microscopy.

* Corresponding author at: National Cancer Institute, NIH, 37 Convent Dr. MSC 4255, Bldg 37 Rm 4032, Bethesda, MD 20892-4255, USA. Tel.: +1 301 435 7843; fax: +1 301 402 0153.
E-mail address: oliveroo@exchange.nih.gov (O.A. Olivero).
[1] These authors contributed equally to this work.

0027-5107/$ – see front matter. Published by Elsevier B.V.
doi:10.1016/j.mrfmmm.2009.03.004

cinogen of moderate potency in mice [10,11] it is important to understand the mechanisms underlying the carcinogenic potential of this drug.

Here, we report for the first time the ability of AZT to act as a centrosome disruptor. By immunohistochemistry (IHC), hamster CHO cells and human NHMEC strains, exposed to AZT for 24 h, showed centrosomal disruption evidenced by pericentrin staining and multipolar mitotic figures, with additional aberrations in tubulin polymerization in cells bearing abnormal centrosomes. In addition, the presence of kinetochore positive micronuclei suggests the potential of the drug to act as an aneugen. The consequences of these events and their occurrence at therapeutic concentrations in human patients remain to be established.

2. Materials and methods

2.1. Culture, exposure and cytotoxicity of normal human mammary epithelial cells (NHMECs)

NHMECs were cultured from organoids derived from tissues obtained at reduction mammoplasty by the Cooperative Human Tissue Network. The NHMEC strains used here have been previously characterized [18]. Cells were grown at 37 °C in 5% CO_2 and serum free mammary epithelial cell medium (Cambrex, Rockland, ME) supplemented with growth factors, insulin and pituitary extracts (Cambrex). AZT (Sigma–Aldrich Co, St. Louis, MO) was dissolved in phosphate buffered saline (PBS) pH 7.2 (Biosource, Rockville, MD) and the final concentration was calculated from absorbance at 266 nm with a molar extinction coefficient of 11,500. Two NHMEC strains were selected for these experiments, based on their ability to incorporate AZT into DNA [19]. Low incorporator (LI) strain M98040 cells and high incorporator (HI) strain M99005 cells were cultured for 6 passages, grown to 75% confluency and exposed in duplicate for 24 h to 0, 10 or 200 μM AZT. For survival studies, cells were seeded in triplicate, trypsinized, and a fraction of the cell suspension was counted in a Coulter particle counter (Model Z1, Coulter Electronics, Luton, UK). Cell survival was expressed as percentage of viable cells in comparison to the unexposed control.

2.2. Culture, exposure and cytotoxicity of Chinese hamster ovary (CHO) cells

CHO cells, obtained from the American type culture collection (ATCC, Manassas, VA), were cultured in HAM F12 medium (Lonza Walkersville, Inc., Walkersville, MD) and supplemented with 10% fetal bovine serum (ATCC), and antibiotics. For cytotoxicity assays, 75% confluent monolayers of CHO cells were exposed to 0, 200, 400 or 800 μM AZT for 24 h in duplicate experiments and processed as described above. CHO has been the cell line of choice for this study because centrosome reduplication occurs despite blockade of DNA synthesis. With the aim of establishing if normal human cells are affected by NRTI treatment, NHMECs were used. The selection of two NHMECs strains with different abilities to incorporate AZT, due to their TK-1 status aimed to determine the role of AZT in the induction of centrosomal amplification.

2.3. Aberrant mitotic figures in CHO cells

CHO cells, seeded in 4-chamber slides (BD Biosciences, Bedford, MA) at a density of 20,000 cells/well were treated in duplicate experiments with 0, 200, 400 and 800 μM AZT for 20 h. AZT was removed and cells were allowed to progress to mitosis for an additional 4 h. Slides were washed with PBS and fixed with 70% alcohol for 15 min. Scoring of multipolar mitoses and lagging chromosomes was performed in 500 cells stained with Giemsa.

2.4. CHO and NHMEC centrosomal integrity determined by immunohistochemistry (IHC) staining

CHO cells and the two NHMEC strains, HI and LI were seeded in 4-chamber slides. CHO cells were exposed as described above. NHMECs were exposed to 0 and 200 μM AZT for 24 h. For both cell types medium was removed and cells were washed 2 times with PBS and once with PBS-Tween (0.05%). Monolayers were fixed with ice-cold methanol for 30 min at −20 °C, followed by washes with PBS-Tween, and extraction by 0.1% Triton-X100 in 1× PBS for 4 min. Slides were then blocked with 2% BSA in PBS for 1 h. Anti-pericentrin (Covance, Emeryville, CA, 1:300 dilution) and anti-β-tubulin (Sigma–Aldrich, 1:200 dilution) were used as primary antibodies for 2 h at room temperature. Following washes in PBS-Tween, the secondary antibodies, anti-rabbit Alexa 488 (Invitrogen, Carlsbad, CA) for pericentrin, and anti-mouse rhodamine red for tubulin (Invitrogen), were applied for 30 min. DAPI (Invitrogen), was used to visualize DNA [20]. Staining by this procedure will produce blue nuclei (DAPI), red tubulin (rhodamine red) and punctate green centrosomal signals (Alexa 488) throughout the cytoplasm. A total of 1,200 cells with visible centrosomes was scored for each treatment group for both the CHO cells and the NHMEC strains.

2.5. Centrosomal integrity in CHO cells determined by transmission electron microscopy (TEM)

CHO cells seeded in 6-well plates were exposed to 0, 200, 400 and 800 μM AZT for 24 h. After incubation, cells were scraped, collected by centrifugation, fixed for 2 h with 2.5% glutaraldehyde (Polysciences, Inc., Warrington, PA) and post-fixed in 1% osmium tetroxide for 1 h at 4 °C. Cells were then dehydrated by ethyl alcohol, incubated with propylene oxide, and embedded with Spurr's low viscosity embedding mixture (Polysciences, Inc.). Polymerized blocks were obtained after an overnight incubation at 70 °C. Semi-thin sections of 0.5 μm stained with toluidine blue were used to select the best preserved structures which were then further trimmed to 500 Å thin sections, stained with uranyl acetate and lead citrate and observed under a CM 100 Philips electron microscope (TEM) at 80 kV (Core facility, USUHS). Electron micrographs were obtained and scanned for further ultrastructural analysis. Numbers of centrosomes and pericentriolar satellites were counted *in situ*, in the TEM screen at a 10,500× magnification, in predetermined areas identified at low magnification as containing centrioles. In order to avoid counting repeated areas during morphometric analysis, only 1 of the 3 grids was analyzed for each experimental condition, and only 1 of 15 whole sections was studied in each grid [21,22]. A total of 50 untreated cells, 60 cells exposed to 400 μM AZT and 55 cells exposed to 800 μM AZT were scored.

2.6. Aurora A and Aurora B staining in NHMECs

NHMECs cultured in 4-well polystyrene chamber slides were exposed to 0, 10 or 200 μM AZT for 24 h, fixed with ice-cold methanol for 30 min at −20 °C, and washed with PBS-Tween. Cells were permeabilized for 5 min with 0.025% SDS and 0.1% Triton in PBS, washed with PBS-Tween and blocked for 1 h at room temperature (blocking solution: 10% goat serum, 1% BSA, 0.02% sodium azide in PBS) before incubation with: a rabbit polyclonal anti-Aurora A antibody (Cell Signaling Technology, Inc., Danvers, MA) at 1:250 dilution in 1%BSA in TBS solution (Tris buffer saline: 0.05 M Tris–HCl 0.15 mM NaCl, pH 7.6), at 4 °C overnight; or a rabbit polyclonal anti-Aurora B antibody (Abcam, Cambridge, MA) at 1:200 dilution in 1% BSA in PBS/Tween solution at 4 °C, overnight. An anti-rabbit Alexa 488-conjugated antibody (Invitrogen) was used as the secondary antibody at a 1:500 dilution for Aurora A or a 1:400 dilution for Aurora B, for 30 min at room temperature. DAPI was used to visualize DNA. Additionally, percentage of cells in different phases of the mitosis was scored in ∼4000 cells from which 200 NHMEC were mitotic, exposed to 200 μM AZT stained with Aurora B. The star indicates statistical significance ($p = 0.002$) for that group compared with the corresponding unexposed controls.

Table 1
Centrosomal amplification and pericentriolar satellites in CHO cells exposed for 24 h to AZT.

Treatment (AZT μM)	% cells w/aberrant mitotic figures[a,b]	% cells bearing > 2 centrosomes (IHC)[c]	% cells bearing > 2 centrosomes (EM)[d]	%cells w/pericentriolar satellites (EM)[d]
0 (control)	0	0.2	1.1 ± 0.8	0.4 ± 0.2
200	0.8	0.4	NA[e]	NA
400	1.8	1.2	2.8 ± 0.8	4.8 ± 0.5
800	5.3	1.9	4.4 ± 0.5	6.9 ± 0.5

[a] $n = 500$ mitotic figures, including multipolar mitoses and cells bearing lagging chromosomes.
[b] Mean of 2 experiments.
[c] $n = 200$ cells with visible centrosomes.
[d] $n = 50$, 60 and 55 cells with visible centrosomes for 0, 200 and 400 μM AZT, respectively.
[e] NA = not assayed.

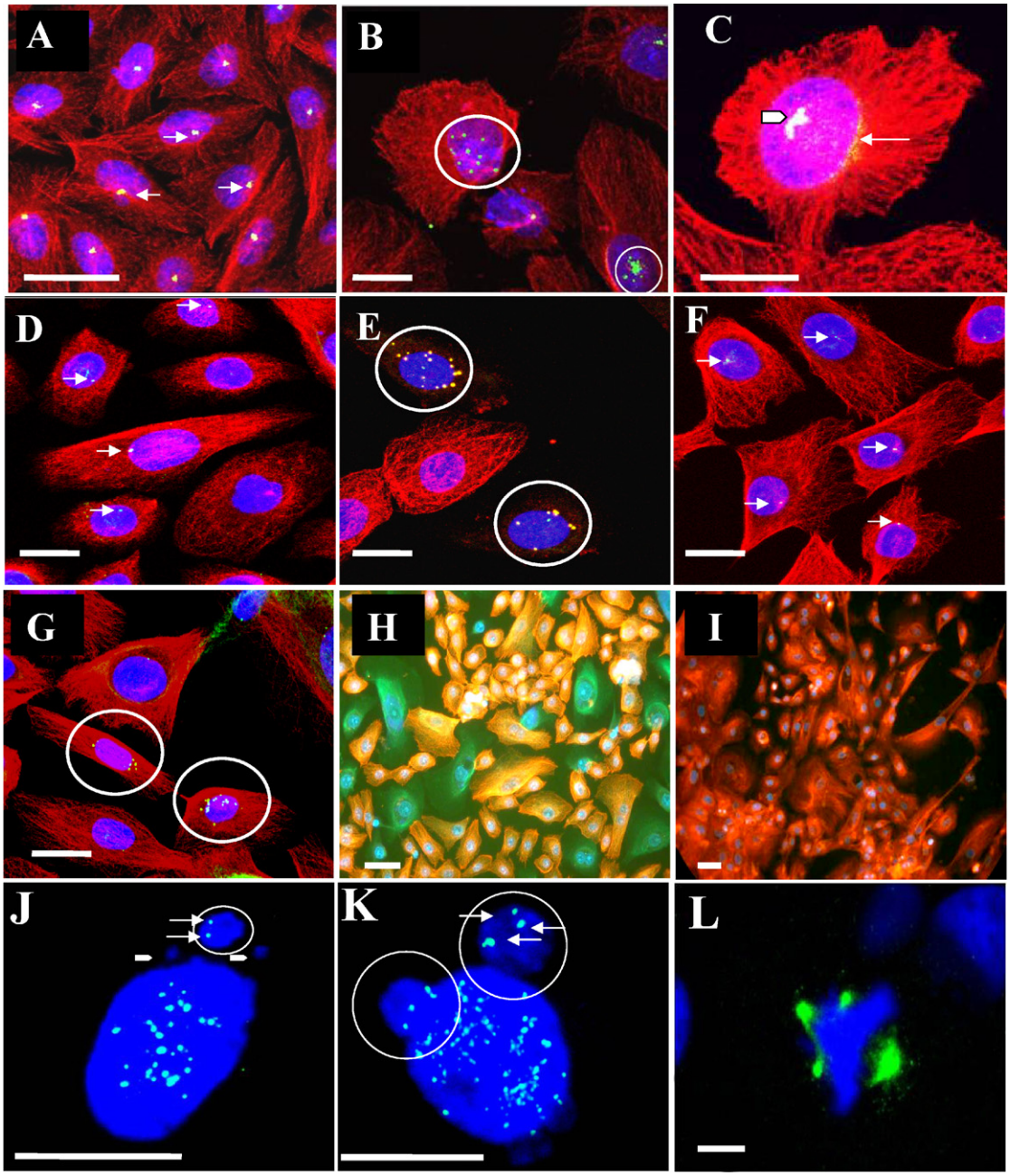

Fig. 1. AZT-exposed CHO cells and NHMEC strains visualized by confocal microscopy. (A–C) CHO cells incubated with anti-pericentrin antibodies (green), anti-β-tubulin antibodies (red), and DAPI to stain DNA (blue). Co-localization of pericentrin and β-tubulin appears yellow. (A) Untreated cells. Arrows indicate the location of centrosomes. (B) CHO cells exposed to 400 μM AZT for 24 h. Circles indicate: centrosomal amplification (top); centrosomal fragmentation multiple pericentrin-positive signals (bottom). (C) CHO cells exposed to 800 μM AZT for 24 h. Arrow head indicates multiple coalescent pericentrin signals; thin white arrow indicates pericentrin aggregation. (D and E) NHMEC HI cells. (D) Untreated cells, arrows indicate centrosomes. (E) Cells exposed to 200 μM AZT for 24 h, circles indicate 2 cells with amplified signal for pericentrin suggesting the presence of multiple centrosomes with co-localizing signal for tubulin. (F and G) NHMEC LI cells. (F) Unexposed cells, arrows indicate centrosomes. (G) Cells exposed to 200 μM AZT for 24 h, circles indicate 2 cells with amplified signal for pericentrin suggesting the presence of multiple centrosomes and normal β-tubulin staining. (H) NHMEC HI cells, stained with anti-β-tubulin antibodies and rhodamine (red); some cells appear green due to the lack of rhodamine staining. (I) NHMEC HI cells, stained as in H but without triton extraction (soluble β-tubulin is retained in cells that have not undergone extraction). The tubulin staining red indicates that green cells in H contained un-polymerized β-tubulin. Bars = 10 μm. (J–L) Kinetochore staining with CREST antibody. (J) CHO cell, exposed to 800 μM AZT for 24 h. Solid arrowheads indicate the presence of 2 small CREST-negative micronuclei, and a white circle indicates a large micronucleus with two CREST-positive kinetochores (white arrows) inside a large micronucleus. (K) NHMEC HI cells showing 2 large circled bodies on top containing kinetochore positive signals (arrows). (L) Triradial spindle revealed by the abnormal multipolar distribution of Aurora A, in a cell treated with 200 μM AZT for 24 h; DAPI (blue) staining shows abnormal multipolar chromosomal distribution. Bars: J–K = 5 μm, L = 1.5 μm.

2.7. CHO and NHMEC kinetochore staining by IHC

CHO cells and NHMECs cultured in 4-well polystyrene chamber slides, were fixed with ice-cold methanol for 30 min at −20 °C and permeabilized for 4 min with 0.1% Triton-X100 in PBS. Then cells were incubated overnight at 4 °C with human anti-kinetochore calcinosis, Raynaud's phenomenon, esophageal dysfunction, sclerodactyly, telangiectasia (CREST) antibody (Antibodies Incorporated, Davis, CA) at a 1:40 dilution in blocking solution. Slides were washed as above and incubated for 90 min at room temperature with anti-human Alexa 488 (Invitrogen 1:500) secondary antiserum in blocking solution (10% goat serum, 0.01% sodium azide, 1% bovine serum albumin in PBS). DAPI was used to visualize nuclei and micronuclei [23]. Scoring of 1000 cells per treatment allowed identification of micronuclei with or without kinetochore (CREST) positive green signals.

2.8. Fluorescent and confocal microscopy

For fluorescence microscopy, cells were visualized and analyzed using a Nikon Eclipse E-400 (Nikon, Inc., Melville, NY) microscope fitted with a Plan Apo 100× objective with a 1.40 numerical aperture. Stained cells were photographed on a Zeiss Axiovert 100 M microscope equipped with a Zeiss Plan Apochromat 100×/1.4 oil Dichromic objective. Confocal images were generated using a Zeiss LSM 510 scanning laser microscope. The LSM 510 zoom software was used to produce a final magnification of 2000×. Images shown are three-dimensional maximal projections generated from a series of images through the *Z*-plane.

2.9. Flow cytometric analysis of NHMEC cell cycle in cells with abnormal tubulin polymerization

NHMECs, exposed to 10 and 200 μM AZT for 24 h in T75 flasks, were trypsinized and pelleted by centrifugation at 860 × *g* for 5 min. Fixation was accomplished by adding ice-cold methanol to pre-chilled cells with gentle vortexing, incubation on ice for 30 min and then centrifugation and resuspension in 0.5% BSA for 10 min at room temperature. Anti-β-tubulin antibody (1:25 dilution, Cell Signaling Technology, Inc.) was added and suspensions incubated for 60 min at room temperature. After washing and spinning, cells were incubated with Alexa Fluor 488 goat anti-rabbit IgG (H + L) (Invitrogen) at a 1:1000 dilution for 30 min at room temperature. Finally, cells were washed, incubated with RNAse (Qiagen, Valencia, CA) and stained with propidium iodide 10 μg/ml (Sigma–Aldrich) at 4 °C, overnight. Cells were analyzed on a FACSCalibur flow cytometer (BD Biosciences, San Jose, CA) using the doublet discrimination module. Data were acquired using CellQuest Pro (BD Biosciences) software. The cell cycle was modeled using ModFit software (Verity Software, Topsham, ME) and tubulin was measured using FlowJo software (TreeStar, Ashland, OR).

2.10. Statistical analysis

Results were expressed as mean ± S.E. of three separate experiments unless otherwise indicated. The Student's *t*-test was used for statistical analysis for the scoring of centrosomal amplification by EM, and ANOVA was used to obtain statistical significance in percentage of mitotic phases in CHO cells.

3. Results

3.1. Cytotoxicity and aberrant mitotic figures in CHO cells

For CHO cells, survival was 81.0, 71.5 and 67.5% at 24 h of exposure for 200, 400 and 800 μM AZT, respectively. Analysis of abnormal mitotic figures was carried out in CHO cells grown in 0, 200, 400, and 800 μM AZT for 20 h, and then grown in AZT free media for 4 h to permit entry into mitosis. An increase in the presence of aberrant cells, including multipolar metaphases/anaphases and cells bearing lagging chromosomes was observed in correlation with increasing doses of AZT. Table 1 shows the scoring of 500 Giemsa-stained cells. There were no abnormal cells in the unexposed cultures, and average percentages of 0.8, 1.8, and 5.3% of cells with aberrant mitotic figures were found in cultures exposed in duplicate experiments to 200, 400, and 800 μM AZT, respectively.

3.2. Centrosomal abnormalities in CHO cells determined by IHC

When compared to untreated CHO cells (Fig. 1A), CHO cells exposed to 200 μM AZT for 24 h showed an increase in the number of pericentrin-positive structures (Fig. 1B and C). Moreover, multiple signals of smaller size were observed in some cells (Fig. 1C) and defined as centrosomal fragmentation. Centrosomal abnormalities were observed in cells exposed to all doses of AZT, and were frequently accompanied by an aberrant aggregation of tubulin (red) (Fig. 1C, thin arrow). Additionally a third type of aberrant centrosomal structure involving multiple centrosomes associated together was defined as aggregation (Fig. 1C arrow head). Scoring for cells containing >2 centrosomes is presented in Table 1. Untreated cells had 0.2% of cells bearing the abnormality, while values for abnormal cells reached 0.4, 1.2, and 1.9% in cells exposed to 200, 400, and 800 μM AZT, respectively.

Amplification of CHO cell centrosomes was confirmed by visualization of EM images. Fig. 2 shows photomicrographs that are representative of multiple images captured and analyzed. Panel A shows cells exposed to 400 μM AZT for 24 h, where black arrows point to centrioles embedded in a proteinaceous pericentriolar matrix. The photos are from an area of cytoplasm close to the nucleus and contain 3 centrioles. Centrioles show cross-sectional microtubule disposition, or cylindrical longitudinal and oblique orientation. Numerous small round electro-dense structures are also observed (B, white arrow head and insert). These are considered to be pericentriolar satellites, non-membranous organelles located close to the centrosome, which in some cases have organized distribution in a semicircle. Panel B shows cells exposed to 800 μM AZT for 24 h. The centrioles (5) are indicated by black arrows and pericentriolar satellites are indicated by white arrowheads.

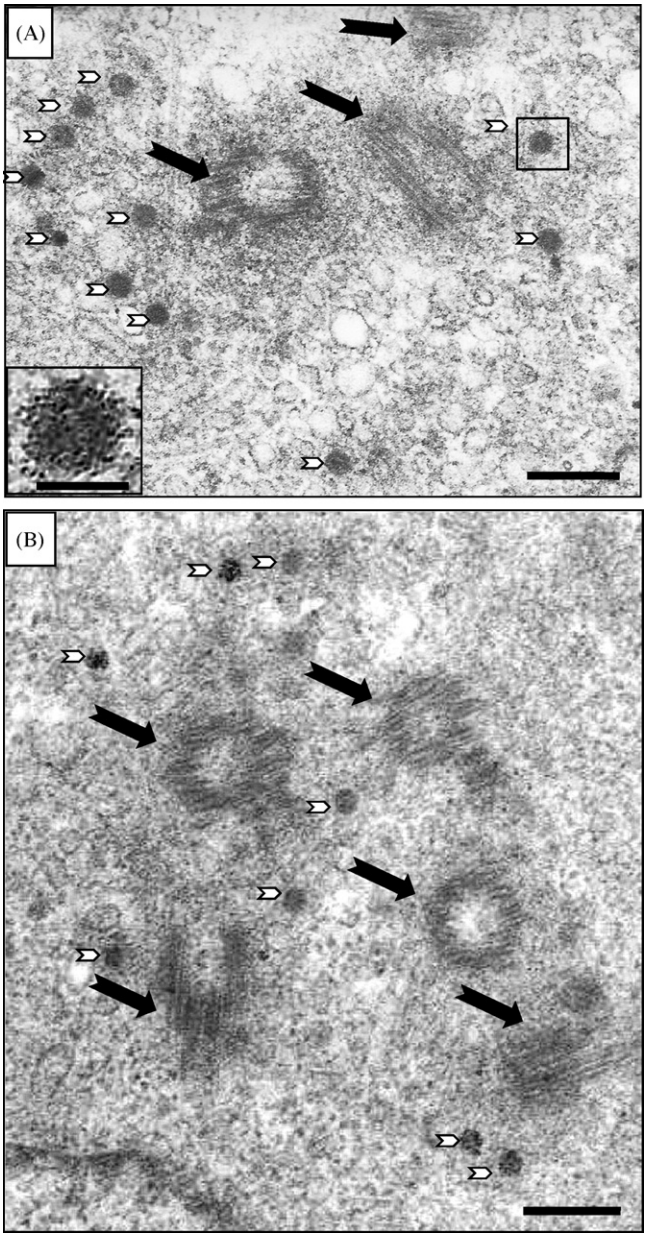

Fig. 2. Electronmicroscopic images of CHO cells. (A) CHO cells exposed to 400 μM AZT for 24 h. Black arrows indicate three centrioles in cross-section or cylindrical and/or oblique orientation. Numerous small round electro-dense structures are also observed (white arrowheads). Boxed insert: detail of small round electro-dense structure. (B) CHO cells exposed to 800 μM AZT for 24 h; centrioles indicated by black arrows and pericentriolar electro-dense bodies with irregular distribution are indicated by white arrowheads. Picture bars = 200 nm, insert bar = 70 nm.

Scoring of 75 EM photos/treatment showed an increase in centrosome number in relation to the AZT concentration. These are

Table 2
Cytotoxicity, centrosomal amplification and abnormal distribution of tubulin in NHMEC strains M99005 (HI cells) and M98040 (LI cells).

AZT μM	% viable cells		% cells bearing > 2 centrosomes[a,b]		% cells with abnormal tubulin distribution (tubulin −)[c]	
	LI	HI	LI	HI	LI	HI
0	100	100	5.3 ± 1.0	6.3 ± 1.0	3.8	3.5
10[a]	84.9 ± 1.0	83.7 ± 5.8	8.0 ± 1.3	14.8 ± 1.5	8.3	21.6
200[b]	83.7 ± 2.0	74.3 ± 10.0	12.2 ± 1.6	21.3 ± 2.3	3.8	23.2

[a] Mean of 4 experiments (n = 200 cells w/visible centrosomes).
[b] Mean of 3 experiments (n = 200 cells w/visible centrosomes).
[c] Mean of 2 experiments (n = 1000 cells).

defined as supernumerary centrosomes in (Table 1) and varied from 1.1 ± 0.8% in unexposed cells to 2.8 ± 0.8% and 4.4 ± 0.5% for 400 and 800 μM AZT, respectively ($p < 0.001$). The percentage of cells showing pericentriolar satellites (Table 1), the specific electron-dense round oval structures associated with the centrosomes, also increased with AZT dose to: 4.8 ± 0.5% and 7.0 ± 0.5% for 400 and 800 μM AZT, respectively ($p < 0.02$), compared with 0.4 ± 0.2% in unexposed cells ($p < 0.001$).

3.3. Centrosomal abnormalities induced in NHMECs

Two NHMEC strains LI and HI were chosen for these experiments, based on their different abilities to incorporate AZT into DNA when exposed to 200 μM AZT for 24 h. At the doses used, 10 and 200 μM, cytotoxicity was very low, with a viability of ~85% for both cell strains when exposed to the highest dose for 24 h (Table 2).

NHMECs were stained with pericentrin, as described above for CHO cells, to identify centrosomal amplification and the results are shown in Table 2 and Fig. 1D–G. pericentrin-positive signals were scored for the total number of cells with visible centrosomes observed in both NHMEC HI and LI strains. HI cells bearing >2 centrosomes were 6.3, 14.8, and 21.3% of cells exposed to 0, 10, and 200 μM AZT, respectively (Table 2). Fig. 1D shows unexposed HI cells, and Fig. 1E shows HI cells exposed to 200 μM AZT. LI cells bearing >2 centrosomes were 5.3, 8.0, and 12.2% of cells exposed to 0, 10 and 200 μM AZT, respectively (Table 2). Fig. 1F shows unexposed LI cells and Fig. 1G shows LI cells exposed to 200 μM AZT.

3.4. β-Tubulin distribution in NHMECs with centrosomal amplification

In addition to centrosomal amplification, some NHMEC cells exposed to 200 μM AZT exhibited a decreased signal for β-tubulin (Fig. 1E). These cells were labeled pericentrin (+)/β-tubulin (−). Cells with normal distribution of tubulin and multiple pericentrin signals, were labeled pericentrin (+)/β-tubulin (+). It would be important to emphasize here that the nomenclature (+) or (−) refers to the lack of visible red signal in the cytoplasm and not to the lack of tubulin in the cell. An apparent lack of β-tubulin staining was observed in a large proportion of AZT-exposed LI and HI NHMECs showing centrosomal amplification. Fig. 1E (circles) shows two cells with multiple pericentrin-positive bodies that lack the red signal for β-tubulin. In these cells the tubulin and pericentrin signals co-localize, as determined by the yellow signals at the centrosome. Scoring of pericentrin (+)/β-tubulin (−) cells was performed using both NHMEC strains (Table 2), and β-tubulin (−) cells appeared stained green due to lack of red signal for β-tubulin (Fig. 1H). In the HI cells there was an increase in β-tubulin (−) cells from 3.5% in the unexposed cells to 23.2% in the AZT-exposed cells. In contrast, in the LI cells the percentage of β-tubulin (−) cells did not differ between AZT-exposed and unexposed cells (Table 2).

In order to understand the nature of the aberrant tubulin staining, fixed AZT-exposed cells that had not been extracted with Triton were processed for immunohistochemistry using the anti-

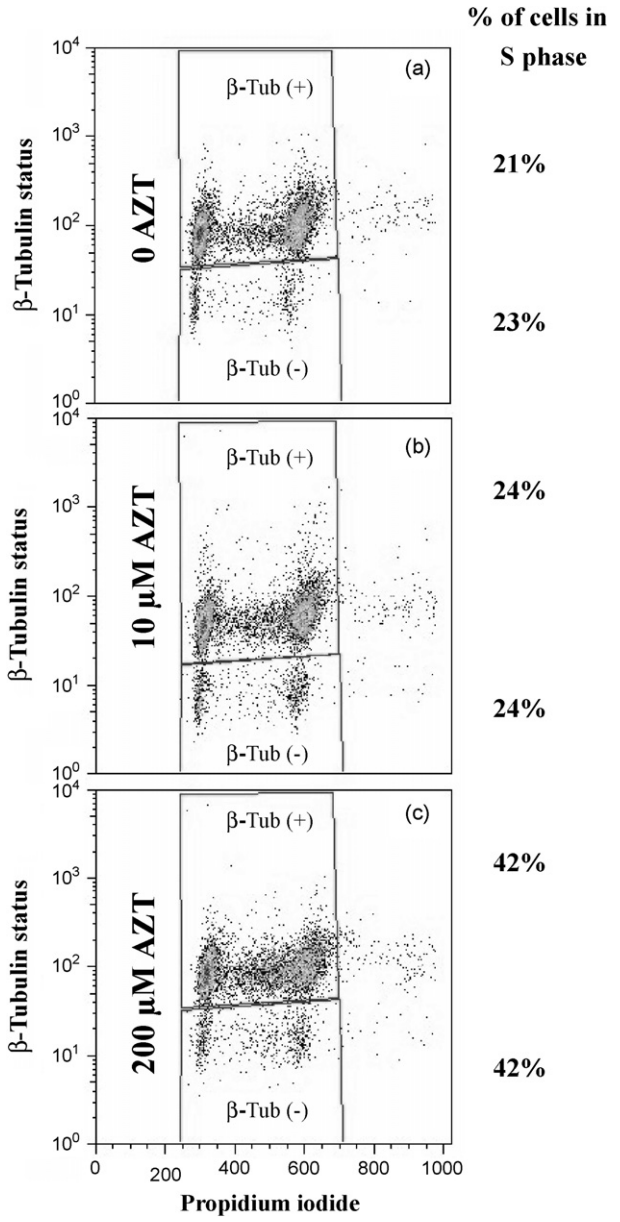

Fig. 3. Flow cytometry of β-tubulin (+) and β-tubulin (−) NHMEC HI cells: (a) unexposed, (b) exposed to 10 μM AZT and (c) exposed to 200 μM AZT. Percentage of cells in S phase for both populations (top and bottom of each panel) is shown on the right. Both β-tubulin (+) and β-tubulin (−) populations show an increase in the percentage of cells in S-phase compared to unexposed controls. Cells deprived of β-tubulin staining, (bottom of each panel) and cells with positive β-tubulin staining, (top of each panel) exhibit similar patterns of distribution.

Table 3
Frequency of micronuclei in CREST (+) and CREST (−) CHO cells and NHMECs[a].

	CHO		NHMEC-LI		NHMEC-HI	
	CREST (+)	CREST (−)	CREST (+)	CREST (−)	CREST (+)	CREST (−)
Control	20.0	2.0	4.0	0	12.0	2.0
AZT 10 μM	NA[b]	NA	13.0	8.0	16.0	6.0
AZT 200 μM	25	6.0	17.0	7.5	30.5	13.0
AZT 400 μM	18.5	5.5	NA	NA	NA	NA
AZT 800 μM	63	17	NA	NA	NA	NA

[a] A total of 6 slides and 2000 cells, in two independent experiments were scored. Values are expressed as number of cells containing either CREST (+) or CREST (−) micronuclei/1000 cells.
[b] NA = not assayed.

β-tubulin antibody. Typically Triton extraction will leave intact a system of microfilamentous bundles and the detergent-resistant cytoskeleton [24]. Two possible outcomes were expected from this experiment: (1) un-polymerized β-tubulin could be retained in the cytoplasm of un-extracted cells and appear as a diffuse red staining, or (2) the absence of all β-tubulin (either polymerized or un-polymerized) would result in unstained cells. In Fig. 1I, a group of un-extracted AZT-exposed HI cells shows a diffuse positive staining for β-tubulin (red color), indicating that the defect previously observed was based on inability of the protein to polymerize and not due to its absence. Hence the un-permeabilized cells retained un-polymerized tubulin and were stained with a faint red color (Fig. 1I).

3.5. Cell cycle profile in pericentrin (+)/β-tubulin (−) cells

Flow cytometry was used to separate pericentrin (+)/β tubulin (−) and pericentrin (+)/β-tubulin (+) cells found in AZT-exposed and unexposed LI and HI NHMECs. The results presented here (for HI cells only, Fig. 3) revealed that the cell cycle in pericentrin (+)/β-tubulin (−) cells is identical to that exhibited by pericentrin (+)/β-tubulin (+) cells from the same culture. This observation is true for the unexposed cells (Fig. 3a), cells exposed to 10 μM AZT (Fig. 3b) and cells exposed to 200 μM AZT (Fig. 3c). Both β-tubulin (+) and β-tubulin (−) populations, represented on the top and bottom of a, b and c panels of Fig. 3 exhibited similar patterns of distribution. Fig. 3 (right side) also shows values for percentages of cells in S-phase, and it is evident that both β-tubulin (+) and β-tubulin (−) cultures exposed to 200 μM AZT had an increase in the percentage of cells in S-phase compared to unexposed controls, as previously reported [9]. Both β-tubulin (+) and β-tubulin (−) cells in S-phase were 24% with 10 μM AZT and 42% with 200 μM AZT. The control values were 21 and 23% for β-tubulin (−) and β-tubulin (+), respectively.

3.6. Aneuploidy assessed by kinetochore (CREST) positive micronuclei in CHO cells and NHMECs

Micronuclei induced by AZT in CHO cells and NHMECs were scored in 1000 cells of both cell types. From those, a subset of micronuclei was found to contain kinetochore (CREST) positive signals. Fig. 1J shows a CHO cell exposed to 800 μM AZT with a kinetochore-bearing micronucleus. NHMECs HI cells exposed to 200 μM AZT are illustrated in Fig. 1K. A kinetochore-bearing micronucleus is observed as blue (DAPI) circles containing multiple green (CREST antibody) signals, additionally Fig. 1K shows a different type of aberration consisting of a large body still attached to the nucleus containing 3–4 CREST positive signals. Values for the frequency of CREST positive micronuclei are shown in Table 3. An increase in the number of micronuclei from 20 to 50/1000 cells was observed in CHO cells with increasing doses of AZT, however, the increase in total of CREST positive containing micronuclei was only significantly different from the controls at the highest dose of 800 μM. In contrast, NHMEC scoring demonstrated significant increases in CREST positive micronuclei in AZT-exposed LI and HI cells at both doses (Table 3).

3.7. Aurora A, Aurora B and multipolar spindles in NHMECs

In addition to the evaluation of centrosomal amplification, the distribution of the centrosomal kinases Aurora A and B was examined by immunohistochemistry. NHMECs exposed to 0, 10 and 200 μM AZT for 24 h were stained with anti Aurora A and B antibodies. Multipolar spindles and multiple centrosomal bodies were

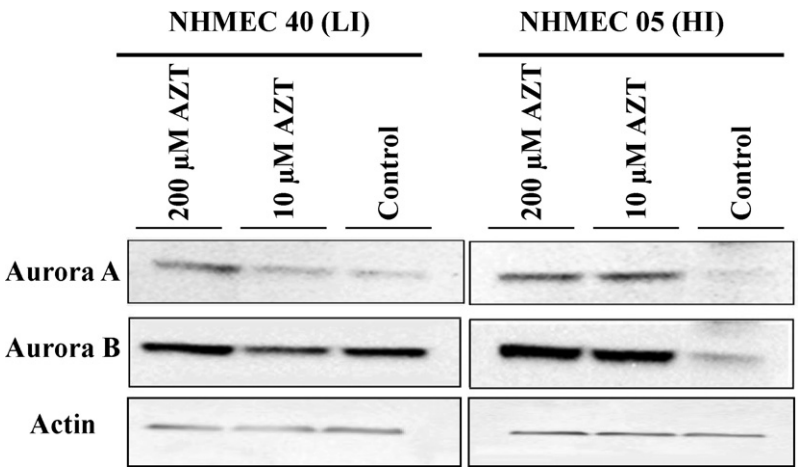

Fig. 4. Western blots for Aurora A and Aurora B proteins in NHMECs. Western blot of NHMECs LI cells (left) and HI cells (right), exposed to 0, 10 and 200 μM AZT for 24 h. Antibodies used to determine protein expression: top panel Aurora A, middle panel Aurora B and bottom panel actin.

Table 4
Distribution of mitotic phases in NHMEC HI and LI cells exposed to 0, or 200 μM AZT for 24 h.

	Prophase	Metaphase	Anaphase	Telophase	Total mitosis[a]
HI control	15.3 ± 1.9	4.0 ± 1.0	3.5 ± 0.9	18.3 ± 2.1	41.0 ± 3.1
HI AZT	24.9 ± 2.5*	3.7 ± 1.0	2.7 ± 0.8	18.7 ± 2.1	50.0 ± 3.4**
LI control	22.6 ± 2.3	5.2 ± 1.1	2.5 ± 0.8	16.9 ± 2.0	47.2 ± 3.3
LI AZT	21.6 ± 2.3	4.2 ± 1.0	2.7 ± 0.8	15.4 ± 1.9	44.0 ± 3.2

[a] Total cells scored ~4000/strain/treatment, total mitotic figures scored = 200/strain/treatment.
* $p = 0.002$.
** $p = 0.016$.

observed in AZT-exposed NHMEC HI cells and were identified by Aurora A-positive signals in NHMECs exposed to 200 μM AZT (Fig. 1L) and 10 μM AZT compared to unexposed controls. Unexposed cells exhibited an average of 6.5% abnormal cells (with >2 Aurora positive signals or multiple spindles) while 14.6% of cells exposed to 10 μM AZT and 21.7% of 200 μM cells were abnormal. A Western blot analysis of NHMEC lysates (Fig. 4) revealed an increase in protein expression of Aurora A in HI cells with both 10 and 200 μM AZT, while in LI cells, there is a modest increase in expression induced by the high dose only. Similarly, Western blot analysis performed with Aurora B revealed a clear increase of the expression of the kinase in HI treated cells with both AZT doses (Fig. 4, right panel) while LI cells did not show a change in the expression level with any dose (Fig. 4, left panel).

Aurora B-stained NHMECs revealed such abundant distribution of the protein that quantitation and comparison among treatments was impossible. Nonetheless mitotic figures were scored and identified by their characteristic pattern (Table 4). Percentage of cells in prophase, metaphase, anaphase and telophase was based on observation of 2000 cells and shown for both cell strains. A statistically significant difference in the percentage of NHMEC HI cells in prophase (25%) was revealed in cells exposed to 200 μM AZT compared to 15% in unexposed cells ($p = 0.002$). NHMECs in LI cells did not show any significant changes in the distribution of mitotic figures. Similarly the rest of the phases analyzed for HI cells did not show statistical significant differences (Table 4).

4. Discussion

The highly effective nucleoside reverse transcriptase inhibitor AZT is a DNA replication chain terminator that induces genomic instability, cell cycle arrest, micronuclei, sister chromatid exchanges, and shortened telomeres [10]. Here we report a novel centrosomal amplification and fragmentation that occurs both in hamster and human cells and results in chromosome missegregation and aneuploidy. The ability of AZT to induce these types of aberrations is reported here for the first time in studies that employed both hamster (CHO) and human NHMECs.

In CHO cells, in addition to centrosomal fragmentation and amplification the presence of numerous pericentriolar satellites was observed. Pericentriolar satellites are described as electrodense bodies associated with the centrosome [25] and further characterized as rich in the centrosomal protein pericentriolar material-1 (PCM-1), having a potential role in centrosomal replication [26]. Inhibition of PCM-1 with specific antibodies revealed that the protein plays an important role in cell cycle regulation, fulfilling an essential function for cells to complete interphase [27].

Incorporation of AZT into NHMEC-DNA and characterization of the incorporators has been documented previously [19]. The deficient incorporation on LI is due to the inactivation of thymidine kinase-1 (TK-1), the enzyme needed for the initial phosphorylation of AZT. However, mitochondrial TK-2 mediated phosphorylation could have occurred facilitating AZT–DNA incorporation under the level of detection of the radioimmunoassay used in the experiments. NHMECs treated with 200 μM AZT for 24 h exhibited an increase in the number of centrosomes, identified by positive pericentrin signals. Furthermore, the centrosomes exhibited other anomalies such as aggregation and fragmentation that co-localized with abundant tubulin, a phenomenon that has been interpreted to indicate an altered nucleation capacity [4].

Abnormal chromosomal distribution was observed in CHO and NHMEC cells revealed by the presence of CREST positive micronucleus, (Fig. 1J–K) evidenced by increased positive signal for kinetochores within micronuclei of cells exposed to AZT. This suggests malfunctioning of the mitotic spindle and as a consequence multiple poles, generated by the migration of numerous centrosomes in an aberrant pattern instead of the typical bipolar mitotic spindle. Multipolar spindles were visualized in NHMECs with immunofluorescence staining using Aurora A, a kinase involved in the maturation of the spindle (Fig. 1L). The fact that the cells divide as evidenced by cells in mitosis (Fig. 1L), indicates that in many cases centrosomal amplification does not impair cell division. However, the fact that the mitosis is delayed, indicated by the presence of a significant number of prophase cells, suggests an abnormality in the mitotic process.

Analysis of NHMECs showed disruption of centrosomes, accompanied by abnormal chromosome distribution and aneuploidy as demonstrated by CREST positive micronuclei; and altered ability of tubulin to polymerize. Two different strains of NHMEC were selected for these experiments, HI cells with the ability to incorporate AZT into DNA and LI cells, lacking that capacity. In both cases, cells exhibited centrosomal amplification after 24 h of AZT exposure; however, the LI cells had less prominent centrosomal amplification suggesting that AZT–DNA incorporation could play a role in this abnormality. Additionally, a cytoskeleton disorder manifested by abnormal distribution and polymerization of tubulin was observed in 23% of the HI (Fig. 1H) cells compared to a 3.8% in LI cells exposed to 200 μM AZT. This last phenomenon suggested a correlation between the capacity of AZT to interact with the ability of tubulin to polymerize and the ability of the drug to incorporate into DNA. Cells exhibiting a lack of signal for β-tubulin staining [defined as pericentrin (+)/β-tubulin (−)] were analyzed by flow cytometry and revealed a similar distribution of cells in S-phase to those with normal tubulin signal [pericentrin (+)/β-tubulin (+)], suggesting that cells bearing centrosomal amplification and abnormal β-tubulin staining are able to cycle in a similar fashion to those with a normal β-tubulin staining.

Western blots, carried out with Aurora A and B indicated that in NHMEC, Aurora A and Aurora B protein expression was up-regulated in HI cells treated with both 10 and 200 μM AZT. No change in protein expression was observed for Aurora B in LI cells and a minor change in Aurora A was observed in cells exposed to 200 μM AZT in LI cells (Fig. 4). Dysfunctional centrosomes and insufficient tension at the kinetochore-spindle connection with subsequent mitotic arrest mediated by the Aurora B–Survivin complex have been reported [28]. Furthermore arrest in pro-metaphase has been observed as a consequence of a depletion of Survivin from the Survivin–Aurora B complex by siRNA [29]. Similarly, in our experiments a statistically significant increase in prophase figures was observed (Table 4). Staining NHMECs with Aurora B allowed the identification of cells in different phases of mitosis, and showed a statistically significant increase of cells in prophase in AZT treated HI cells (Table 4). This indicates that although the cells completed mitosis they do it abnormally, most likely due to the arrest induced by an active mitotic check point.

Aneuploidy is an expected consequence of the defects described above. CREST kinetochore positive micronuclei were observed in

CHO cells and NHMECs, however, a peculiar distinction should be mentioned between observations in the two cell types. Although the micronuclei observed in CHO correspond to the classical described micronuclei (separated from the main nucleus, small in size not to exceed 25% of the nucleus), the ones found in NHMEC look somewhat different. Some of them are larger and also show a connection with the main nucleus. They resemble a protrusion of the nucleus rather than a separate body as if the protrusion would culminate in strangulation. Most of them bear CREST positive signals, in many instances, many signals have been visualized (Fig. 1K).

In summary, AZT-induced centrosomal amplification is documented in hamster and human cells for the first time. Mechanistical studies performed with higher drug concentration revealed supernumerary centrosomes as well as pericentriollar satellites. Cells bearing the aberration were able to cycle in a similar fashion as unaffected cells, evidenced by the presence of multipolar mitotic figures. Both, amplification and abnormal mitotic figures were observed in the presence of therapeutically relevant doses of AZT. The presence of kinetochore bearing micronuclei suggests that unbalanced chromosomal segregation or aneuploidy takes place. It could be speculated then that aneuploidy could be one of the mechanisms underlying the carcinogenicity of AZT. Experiments aimed to determine if this is a phenomenon exclusively linked to AZT or shared by different nucleoside analogs are in progress.

Conflict of interest statement

None.

Acknowledgments

The authors would like to thank Dr. Dan Sackett from the Laboratory of Integrative and Medical Biophysics, NICHD, NIH, for guidance and critical reading of the manuscript and Dr. Jean-Marie Peloponese Jr. for advise with the staining. The work was supported, in part, by the Intramural Research Program of the NIH, National Cancer Institute, Center for Cancer Research.

References

[1] S. Doxsey, W. Zimmerman, K. Mikule, Centrosome control of the cell cycle, Trends Cell Biol. 15 (2005) 303–311.
[2] A.B. D'Assoro, W.L. Lingle, J.L. Salisbury, Centrosome amplification and the development of cancer, Oncogene 21 (2002) 6146–6153.
[3] P.E. Carroll, M. Okuda, H.F. Horn, P. Biddinger, P.J. Stambrook, L.L. Gleich, Y.Q. Li, P. Tarapore, K. Fukasawa, Centrosome hyperamplification in human cancer: chromosome instability induced by p53 mutation and/or Mdm2 overexpression, Oncogene 18 (1999) 1935–1944.
[4] W.L. Lingle, W.H. Lutz, J.N. Ingle, N.J. Maihle, J.L. Salisbury, Centrosome hypertrophy in human breast tumors: implications for genomic stability and cell polarity, Proc. Natl. Acad. Sci. U.S.A. 95 (1998) 2950–2955.
[5] G.A. Pihan, A. Purohit, J. Wallace, H. Knecht, B. Woda, P. Quesenberry, S.J. Doxsey, Centrosome defects and genetic instability in malignant tumors, Cancer Res. 58 (1998) 3974–3985.
[6] M.S. Satoh, T. Lindahl, Enzymatic repair of oxidative DNA damage, Cancer Res. 54 (1994) 1899s–1901s.
[7] K. Mikule, B. Delaval, P. Kaldis, A. Jurcyzk, P. Hergert, S. Doxsey, Loss of centrosome integrity induces p38–p53–p21-dependent G_1–S arrest, Nat. Cell Biol. 9 (2007) 160–170.
[8] E.H. Hinchcliffe, F.J. Miller, M. Cham, A. Khodjakov, G. Sluder, Requirement of a centrosomal activity for cell cycle progression through G1 into S phase, Science 291 (2001) 1547–1550.
[9] O.A. Olivero, Mechanisms of genotoxicity of nucleoside reverse transcriptase inhibitors, Environ. Mol. Mutagen. 48 (2007) 215–223.
[10] IARC. Monographs on the Evaluation of Carcinogenic Risks to Humans. Some antiviral and antineoplastic drugs, and other pharmaceutical agents, vol. 76, World Health Organization. International Agency for Research on Cancer, Lyon, France, 2000, pp. 73–127.
[11] O.A. Olivero, L.M. Anderson, B.A. Diwan, D.C. Haines, S.W. Harbaugh, T.J. Moskal, A.B. Jones, J.M. Rice, C.W. Riggs, D. Logsdon, S.H. Yuspa, M.C. Poirier, Transplacental effects of 3′-azido-2′,3′-dideoxythymidine (AZT): tumorigenicity in mice and genotoxicity in mice and monkeys, J. Natl. Cancer Inst. 89 (1997) 1602–1608.
[12] B.A. Diwan, C.W. Riggs, D. Logsdon, D.C. Haines, O.A. Olivero, J.M. Rice, S.H. Yuspa, M.C. Poirier, L.M. Anderson, Multiorgan transplacental and neonatal carcinogenicity of 3′-azido-3′-deoxythymidine in mice, Toxicol. Appl. Pharmacol. 15 (1999) 82–99.
[13] O.A. Olivero, A.M. Tejera, J.J. Fernandez, B.J. Taylor, S. Das, R.L. Divi, M.C. Poirier, Zidovudine induces S-phase arrest and cell cycle gene expression changes in human cells, Mutagenesis 20 (2005) 139–146.
[14] P.A. Escobar, O.A. Olivero, N.A. Wade, E.J. Abrams, C.J. Nesel, R.B. Ness, R.D. Day, B.W. Day, Q. Meng, J.P. O'Neill, D.M. Walker, M.C. Poirier, V.E. Walker, W.L. Bigbee, Genotoxicity assessed by the comet and GPA assays following in vitro exposure of human lymphoblastoid cells (H9) or perinatal exposure of mother-child pairs to AZT or AZT-3TC, Environ. Mol. Mutagen. 48 (2007) 330–343.
[15] O.A. Olivero, J.M. Ming, S. Das, I.L. Vazquez, D.L. Richardson, A. Weston, M.C. Poirier, Human inter-individual variability in metabolism and genotoxic response to zidovudine, Toxicol. Appl. Pharmacol. (2007).
[16] M. Viora, G. Di Genova, R. Rivabene, W. Malorni, A. Fattorossi, Interference with cell cycle progression and induction of apoptosis by dideoxynucleoside analogs, Int. J. Immunopharmacol. 19 (1997) 311–321.
[17] B. Chandrasekaran, T.E. Kute, D.S. Duch, Synchronization of cells in the S phase of the cell cycle by 3′-azido-3′-deoxythymidine: implications for cell cytotoxicity, Cancer Chemother. Pharmacol. 35 (1995) 489–495.
[18] C. Keshava, D. Whipkey, A. Weston, Transcriptional signatures of environmentally relevant exposures in normal human mammary epithelial cells: benzo[*a*]pyrene, Cancer Lett. 221 (2005) 201–211.
[19] O.A. Olivero, J.M. Ming, S. Das, I.L. Vazquez, D.L. Richardson, A. Weston, M.C. Poirier, Human inter-individual variability in metabolism and genotoxic response to zidovudine, Toxicol. Appl. Pharmacol. 228 (2008) 158–164.
[20] J.M. Peloponese Jr., K. Haller, A. Miyazato, K.T. Jeang, Abnormal centrosome amplification in cells through the targeting of Ran-binding protein-1 by the human T cell leukemia virus type-1 Tax oncoprotein, Proc. Natl. Acad. Sci. U.S.A. 102 (2005) 18974–18979.
[21] C. Semino-Mora, H. Liu, T. McAvoy, C. Nieroda, K. Studeman, A. Sardi, A. Dubois, Pseudomyxoma peritonei: is disease progression related to microbial agents? A study of bacteria, MUC2 AND MUC5AC expression in disseminated peritoneal adenomucinosis and peritoneal mucinous carcinomatosis, Ann. Surg. Oncol. 15 (2008) 1414–1423.
[22] M.C. Semino-Mora, M.E. Leon-Monzon, M.C. Dalakas, Effect of L-carnitine on the zidovudine-induced destruction of human myotubes. Part I. L-Carnitine prevents the myotoxicity of AZT in vitro, Lab Invest. 71 (1994) 102–112.
[23] L. Emdad, D. Sarkar, Z.Z. Su, H. Boukerche, M. Bar-Eli, P.B. Fisher, Progression elevated gene-3 (PEG-3) induces pleiotropic effects on tumor progression: modulation of genomic stability and invasion, J. Cell Physiol. 202 (2005) 135–146.
[24] M. Osborn, K. Weber, The detergent-resistant cytoskeleton of tissue culture cells includes the nucleus and the microfilament bundles 4, Exp. Cell Res. 106 (1977) 339–349.
[25] R. Balczon, L. Bao, W.E. Zimmer, K. Brown, R.P. Zinkowski, B.R. Brinkley, Dissociation of centrosome replication events from cycles of DNA synthesis and mitotic division in hydroxyurea-arrested Chinese hamster ovary cells, J. Cell Biol. 130 (1995) 105–115.
[26] A. Kubo, H. Sasaki, A. Yuba-Kubo, S. Tsukita, N. Shiina, Centriolar satellites: molecular characterization, ATP-dependent movement toward centrioles and possible involvement in ciliogenesis, J. Cell Biol. 147 (1999) 969–980.
[27] R. Balczon, C. Simerly, D. Takahashi, G. Schatten, Arrest of cell cycle progression during first interphase in murine zygotes microinjected with anti-PCM-1 antibodies, Cell Motil. Cytoskel. 52 (2002) 183–192.
[28] S.M. Lens, R.H. Medema, The survivin/Aurora B complex: its role in coordinating tension and attachment, Cell Cycle 2 (2003) 507–510.
[29] M. Castedo, J.L. Perfettini, T. Roumier, K. Andreau, R. Medema, G. Kroemer, Cell death by mitotic catastrophe: a molecular definition, Oncogene 23 (2004) 2825–2837.